

In this chapter, the fundamental operating principles of the laser diode are reviewed. The need for a resonant cavity, gain medium and optical confinement are explained. The main radiative recombination and absorption mechanisms are then presented. Optical confinement using a double-heterostructure is examined in conjunction with the concept of population inversion. The main dark (non-radiative) recombination mechanisms (Auger, Shockley-Read-Hall) are explained. Typical behaviour of the L-I curve, beam quality and corrective optics are examined. A brief review of laser structures is given, including that of tapered lasers and VCSELs. Finally, device degradation, lifetime and heat management are reviewed.

2.1 The laser diode

A laser diode in its simplest form consists of a gain medium and an optical cavity. Such a device is depicted in figure 2.1. In the most simple laser diodes, gain is generated by forward biasing a p-n junction until an abundance of both electrons and holes are present in the depletion region. In direct band gap semiconductors, these carriers radiatively recombine via stimulated emission to produce photons. By cleaving the diode, a resonant cavity is formed, the generated photons reflect off the mirrors at either end of the cavity stimulating the emission of more photons. Thus, a high intensity optical field is built up.

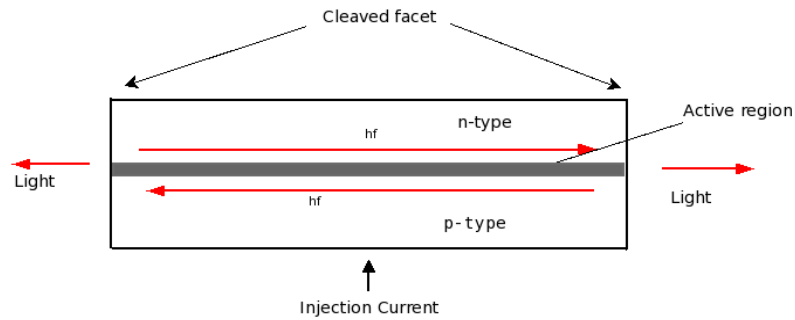


Figure 2.1 : The laser cavity and active gain medium.

2.1.1 Radiative transitions

The key physical process responsible for lasing action is stimulated recombination. Figure 2.2a depicts this process in a direct band gap semiconductor. It shows a photon of energy E_{21} propagating from the left of the picture and interacting with an electron-hole pair. The electron in the conduction band has energy E_2 , and the hole in the valance band has energy E_1 . A second photon of energy $E_2 - E_1 = E_{21} = \hbar \omega$ will be emitted.

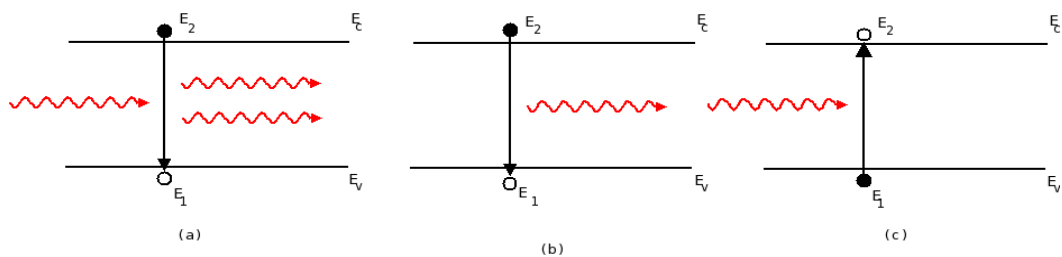


Figure 2.2: The processes of stimulated emission (a), spontaneous emission (b) and absorption (c).

This photon will be of the same frequency, phase and direction as the photon which stimulated the emission. These two photons will stimulate more electrons to fall to

the valance band. In this way a large radiation field of monochromatic coherent light can be built up. The downward transition rate is [1] given by

$$r^{21} = B_{21} f_2 [1 - f_1] P(E_{21}) \quad , \quad (2.1)$$

where B_{21} is the transition probability, f_2 is the probability that energy E_2 is occupied, f_1 is the probability that E_1 is occupied and $P(E_{21})$ is the photon density at energy E_{21} .

Electrons can also spontaneously recombine with holes, thereby emitting a photon.

This is depicted in figure 2.2b. The spontaneous emission rate is given by

$$r^{21}(spon) = A_{21} f_2 [1 - f_1] \quad , \quad (2.2)$$

where A_{21} is the downward transition probability [1]. Photons can also be reabsorbed exciting an electron from the valance band to the conduction band. The upward transition rate r_{12} is written as

$$r^{12} = B_{12} f_1 [1 - f_2] P(E_{21}) \quad (2.3)$$

where B_{12} is the transition probability, f_1 is the probability that state E_1 contains an electron and f_2 is the probability that state E_2 contains an electron. [1] A_{21} , B_{12} and B_{21} are known as the Einstein coefficients and are related to each other by the Einstein relations

$$A_{21} = (8 \pi \bar{n}^3 E_{21}^2 / h^3 c^3) B_{21} \quad (2.4)$$

$$B_{12} = B_{21} \quad (2.5)$$

2.1.2 Population inversion

Above a critical value of injection current, population inversion occurs and stimulated emission dominates absorption. Transparency is defined as the condition when the

probability of stimulated emission is *equal* to the probability of absorption. Gain occurs when the probability of stimulated emission is *greater* than the probability of absorption. Population inversion can be defined as

$$B_{21}f_2[1-f_1] > B_{12}f_1[1-f_2] \quad . \quad (2.6)$$

Expression 2.6 can be understood as the probability of an electron being in the conduction band and a hole being in the valance band having to be greater than the probability of an electron being in the valance band and a hole in the conduction band.

If f_1, f_2 are replaced with the Fermi-Dirac functions for E_1 and E_2 respectively,

$$f_1 = \frac{1}{1 + \exp\left(\frac{E_1 - F_p}{kT}\right)} \quad (2.7)$$

$$f_2 = \frac{1}{1 + \exp\left(\frac{E_2 - F_p}{kT}\right)} \quad . \quad (2.8)$$

then the expression $F_n - F_p > E_2 - E_1$ is obtained. This can be rewritten as $F_n - F_p > E_g$.

Thus, population inversion occurs when separation of the the quasi-Fermi levels is greater than the band gap energy as shown in figure 2.3.

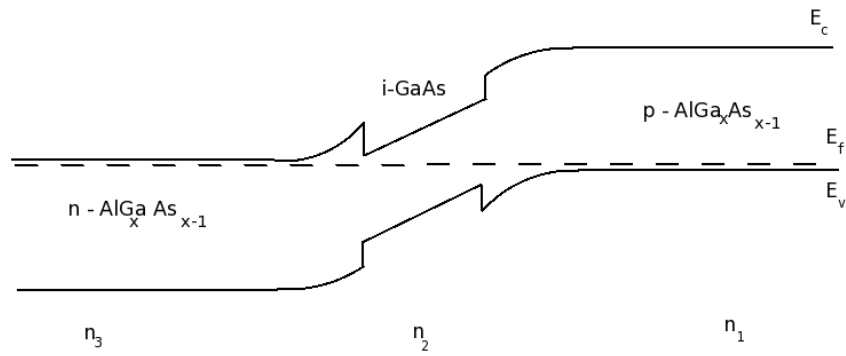


Figure 2.3a: Energy bands at equilibrium in a heterostructure laser.

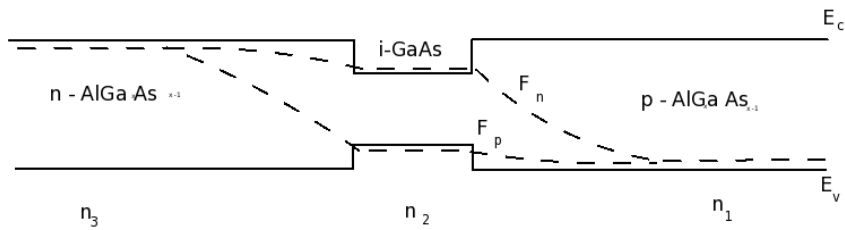


Figure 2.3b: Energy bands at population inversion.

2.1.3 The resonant cavity

The cavity in a laser only supports an integral number of half wavelengths between each mirror, as illustrated in figure 2.4. This is due to the round-trip phase matching condition. The energy difference between the modes (ΔE) can be shown to be

$$\Delta E = \frac{c h}{2 L n_g} \quad , \quad (2.9)$$

where c is the speed of light in a vacuum, n_g is the group index of cavity, h is Plank's

constant, and L is the cavity length. The active region only produces gain over a finite range of energies. Thus only those cavity modes whose wavelength corresponds to this energy range can lase. Figure 2.5 plots the gain profile of a laser with the resonant modes of the cavity. The two vertical lines represent the wavelength range where gain exceeds loss. The short spikes plotted at the bottom of the graph represent modes of the cavity.

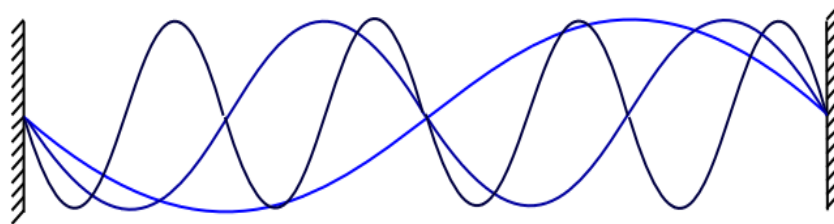


Figure 2.4: Supported cavity modes [2]

Although typically tens of modes experience gain, far above threshold it is not possible for all the modes to lase at once, as they compete with each other. The mode with the greatest net gain (gain minus loss) can stimulate more photons of its frequency than a mode with slightly fewer photons. Thus, the net result is that the mode with the greatest net gain will grow the fastest, taking electron-hole pairs in the gain medium away from the other modes. The result is that one mode dominates and its spectral width is far sharper than one would expect theoretically from the resonant cavity in the absence of gain. (The above discussion neglects filamentation and spectral hole burning effects.)

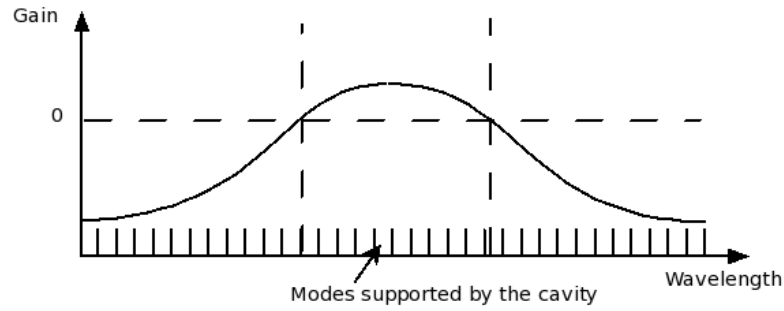


Figure 2.5 Viable lasing modes of the laser, the gain and loss curves have been shown along with the frequencies at which the cavity will resonate, denoted by the vertical lines on the horizontal axis [3].

One mirror of the resonant cavity is usually coated with an anti-reflective coating to enable light to be radiated from only one end of the device. For a laser to lase at a given energy, the material gain $g(E)$, multiplied by the confinement factor Γ must equal all the losses (i.e. internal cavity losses α_i ; and the mirror losses)

$$\Gamma g(E) = \alpha_i + \frac{1}{2L} \ln\left(\frac{1}{R_1 R_2}\right) \quad , \quad (2.10)$$

where L is the cavity length and R_1, R_2 are the power reflectivities of the two mirror facets.

2.2 Separate confinement layers

Early homojunction lasers consisted simply of a p-n junction with no waveguiding or carrier confining structure. This led the optical mode to extend into the bulk and thus optical losses were very high. Consequently, operation was only possible at very large current densities and cryogenic temperatures.

A major step forward was the development of the double-heterostructure laser, depicted in figure 2.6a. In this device, carriers were confined to a thin (70-200nm) layer of material, whose band gap energy was narrower than that of the cladding layer. The confinement region confined the optical mode as well due to its lower refractive index. The next generation of devices used two separate regions (figure 2.6b) - one to confine the carriers and one to contain the optical mode. This enables quasi-independent optimisation of each structure for optimum carrier and light confinement. Such a device is called a separate confinement heterostructure (SCH) laser. If the AlGaAs composition is graded in the wave guiding region better carrier collection efficiency and wave guiding can be achieved (figure 2.6c). This is called the graded index separate confinement heterostructure (GRINSCH) laser [2].

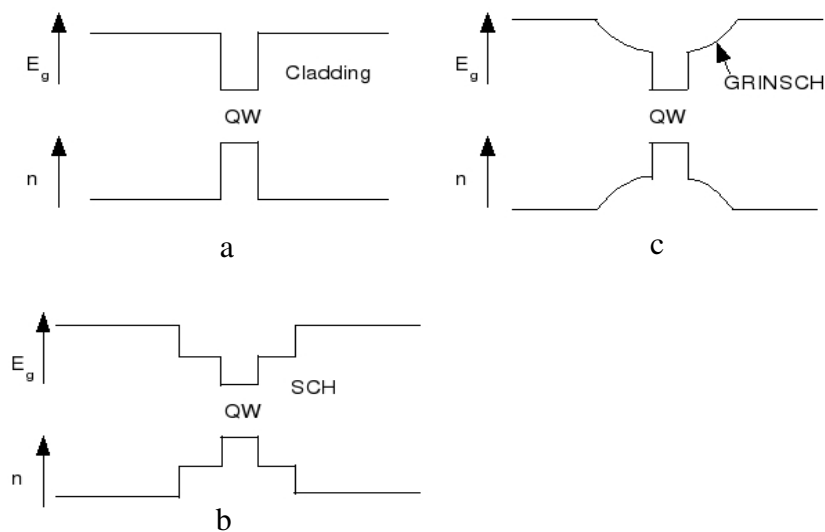


Figure 2.6: Separate confinement of carriers and waveguideing [2].

The optical confinement Γ of a mode is defined as

$$\Gamma = \frac{\int_{-d/2}^{+d/2} I(x) dx}{\int_{-\infty}^{+\infty} I(x) dx} \quad [3,4], \quad (2.11)$$

where I is the modal intensity and d is the width of the active region. Thus, the confinement factor determines the fraction of the optical power of the mode which is confined in the gain material. A plot of the refractive index profile of a double-heterostructure laser is depicted in figure 2.7.

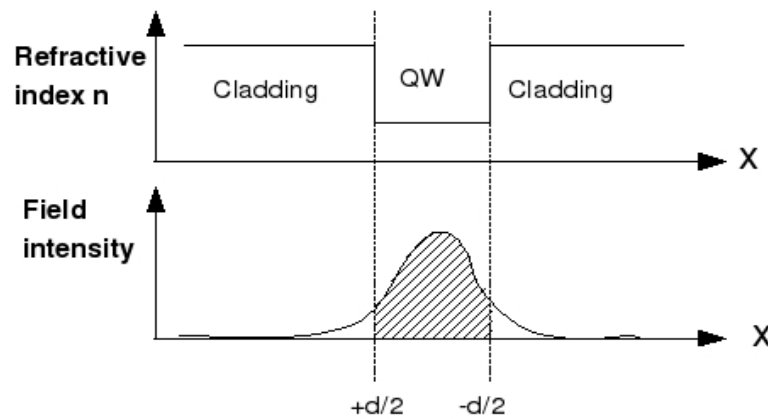


Figure 2.7: Optical confinement [3,4].

2.3 Fundamentals of quantum wells

As described in section 2.2, the QW is one of the most important aspects of a modern laser diode. In this section, the fundamental concepts of the QW will be discussed - quantisation of momentum normal to the plane of the QW and the concept of k-space is reviewed.

2.3.1 Quantum wells and Schrödinger's equation

The width of a quantum well is comparable to the wavelength of an electron. Thus, an analogy can be drawn between an optical waveguide (for photons) and a QW (for electrons). Just as a mode in a waveguide can be described by the wave equation, the wave function of an electron can be described by the time invariant Schrödinger equation [5]

$$\frac{-\hbar^2}{2m^*} \left(\frac{\partial^2}{\partial x^2} + \frac{\partial^2}{\partial y^2} + \frac{\partial^2}{\partial z^2} \right) \psi + V(x, y, z) = E \psi \quad . \quad (2.12)$$

For a 1D structure the equation can be written as

$$\frac{-\hbar^2}{2m^*} \left(\frac{\partial^2}{\partial z^2} \right) \psi + V(z) = E \psi \quad . \quad (2.13)$$

An ideal and infinite quantum well can be described as a region of 0 potential surrounded by a region of infinite potential. Such a situation is depicted in figure 2.8.

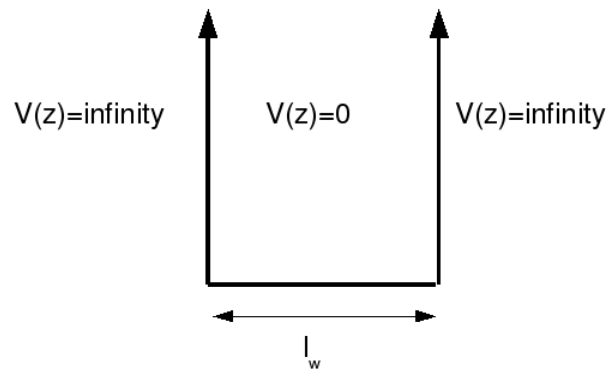


Figure 2.8: Infinite quantum well [5].

Equation 2.13 can be recognised as a wave equation, as such a known solution is of the form

$$\psi(z) = A \sin(k_z z) + B \cos(k_z z) \quad . \quad (2.14)$$

Substituting this wavefunction into Schrödinger's equation gives [5]

$$\frac{\hbar^2 k^2}{2m^*} (A \sin(k_z z) + B \cos(k_z z)) = E (A \sin(k_z z) + B \cos(k_z z)) \quad , \quad (2.15)$$

resulting in

$$\frac{\hbar^2 k_z^2}{2m^*} = E \quad . \quad (2.16)$$

The potential well is infinite so the electron cannot escape from it. If the left hand side of the well is taken as the origin, then B must equal 0. For the probability function to go to zero at the right hand side of the well, the following relation must hold

$$k_z = \frac{\pi n}{l_w} \quad , \quad (2.17)$$

where, n is an integer. Thus, the wave vector k_z is a discrete function normal to the plane of the QW. The energy of the subband is then given by

$$E_n = \frac{\hbar^2 \pi^2 n^2}{2m l_w^2} \quad . \quad (2.18)$$

The only constant left to find in equation 2.14 is A. If the wave is a probability function and it is known that the electron is somewhere within the energy level, ψ can be normalised to 1,

$$\int_0^{l_w} \psi^*(z) \psi(z) dz = 1 \quad [6] \quad (2.19)$$

resulting in

$$A = \sqrt{\frac{2}{l_w}} \quad . \quad (2.20)$$

Thus, the wave function can be evaluated as

$$\psi_z(z) = \sqrt{\frac{2}{l_w}} \sin\left(\frac{\pi n z}{l_w}\right) . \quad (2.21)$$

Figure 2.9 depicts the first three solutions of equation 2.21 for an infinite QW.

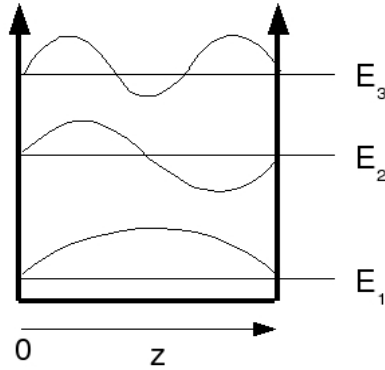


Figure 2.9: Wave function [7].

Although the electron wave function has discretised k -vectors, the electrons are free to move in the 2D plane parallel to the well, whereby the square of the wave vector parallel to the plane is

$$\mathbf{k}_{xy}^2 = \mathbf{k}_x^2 + \mathbf{k}_y^2 , \quad (2.22)$$

and using the operator $\mathbf{p} = \hbar \mathbf{k}$ for momentum. The total energy of a confined electron can be written as the sum of the energy contributed from the confined z -momentum and that from the 2D momentum i.e.

$$E_e(\mathbf{k}) = E_n + \frac{\hbar^2 k_e^2}{2m_c^*} . \quad (2.23)$$

The quantum well of a laser diode is engineered to produce a quantum well in both the conduction and valence bands, see figure 2.10.

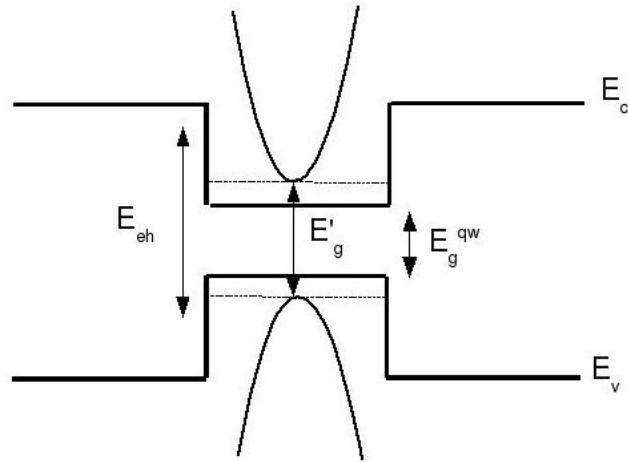


Figure 2.10: Conduction and valance band.

For an electron and hole to radiatively recombine via stimulated emission, both carriers must have exactly the same momentum ($k_h=k_e$), because no momentum can be given to the photon. Thus, for a direct band gap transition between two carriers with the same momentum a photon of energy

$$E_{eh}(\mathbf{k}) = E'_g + \frac{\hbar^2 k_h^2}{2m_v^*} + \frac{\hbar^2 k_e^2}{2m_c^*} = E'_g + \frac{\hbar^2 k^2}{2m_r^*} \quad (2.24)$$

would be released. Here E'_g is defined as the sum of the band gap of the QW (E_g^{qw}) plus the offset of the both (electron and hole) subband energies. The reduced mass m_r is given as

$$m_r^* = \frac{m_c^* m_v^*}{m_c^* + m_v^*} . \quad (2.25)$$

In the above derivation, it has been assumed that the QW is infinite. If the well is not infinite, the wave functions will extend into the barrier. It has also been assumed that the bands are parabolic and symmetrical in all directions.

2.3.2 3D and 2D k-space

Although it was implied in the previous section that the wavefunction only has a quantised wave vector in the plane normal to the QW, quantised wavefunctions exist in all directions of the crystal. This can be demonstrated if a wavefunction $\psi(x) = A \sin(k_x x)$ within a 3D crystal is considered. The wavefunction must tend to zero at the bounds of the crystal ($x=0, L_x$). Thus [7]

$$\sin(k_x \cdot 0) = \sin(k_x \cdot L_x) = 0 \quad . \quad (2.26)$$

As in the previous section, it is clear from equation 2.26 that all the electron wavefunction must have a discrete set of k_x vectors i.e.

$$k_x = \frac{\pi n}{L_i} \quad , \quad (2.27)$$

where n is the quantum number of the system. A set of electron states is given by [7]

$$\mathbf{k} = n_x \mathbf{K}_x + n_y \mathbf{K}_y + n_z \mathbf{K}_z \quad , \quad (2.28)$$

where

$$|\mathbf{K}_i| = \pi / L_i \quad . \quad (2.29)$$

The set of 3D states is depicted in figure 2.11. If one of the dimensions of the crystal system is reduced (as in a QW), then equation 2.27 shows that the 3D density states spreads out, forming planes of 2D states. This is depicted in figure 2.12.

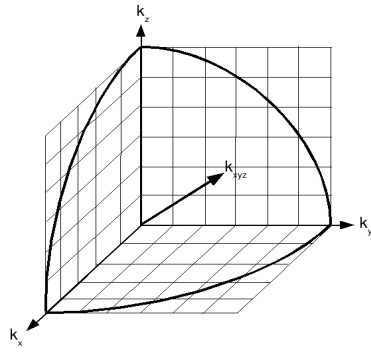


Figure 2.11: 3D density of states [7]

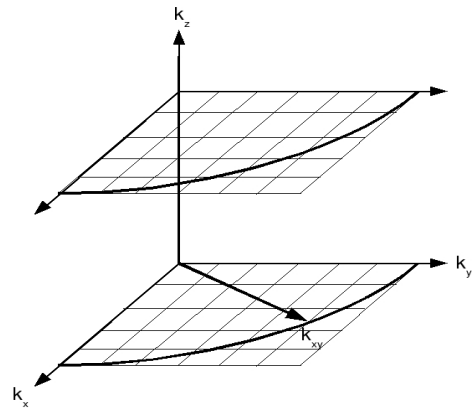


Figure 2.12: 2D density of states [7].

It can be shown [7] that the total number of states in an m dimensional system is

$$N_s = \frac{V_k}{(2\pi/L_m)^m} \quad , \quad (2.30)$$

where $m=1, 2, 3$ and L_m is the length of each dimension of the crystal in real space.

The density of states is defined as

$$\int_{V_k} \rho^{\text{mD}}(k) d^3 k = \frac{N_s}{V} \quad (2.31)$$

where ρ^{mD} is an m dimensional density of states function and V is the crystal volume.

Solving equation 2.31 and using equation 2.30 gives

$$\rho^{\text{mD}}(k) \equiv \frac{1}{V} \frac{dN_s}{dk} = \frac{(L)^m}{V} \frac{1}{(2\pi)^m} \frac{dV_k}{dk} \quad . \quad (2.32)$$

This expression is also valid for non-parabolic bands.

By multiplying by the density of states by the occupational probability $f(k)$ and

integrating, the number of carriers in each subband can be calculated as

$$c_i = 2 \int_0^{\infty} \rho(k) f(k) d^3 k \quad (2.33)$$

The factor of two is included to take account of spin degeneracy. Assuming one quasi-Fermi level for all the sub bands, (i.e. all subbands are in equilibrium with each other), the total carrier density for all the bands in the QW can be calculated as

$$c = 2 \sum_{i=1}^N \int_0^{\infty} \rho(k) f(k) d^3 k \quad (2.34)$$

where N is the number of bands. A figure depicting the 2D-density of states and the structure of the subbands is shown in figure 2.13.

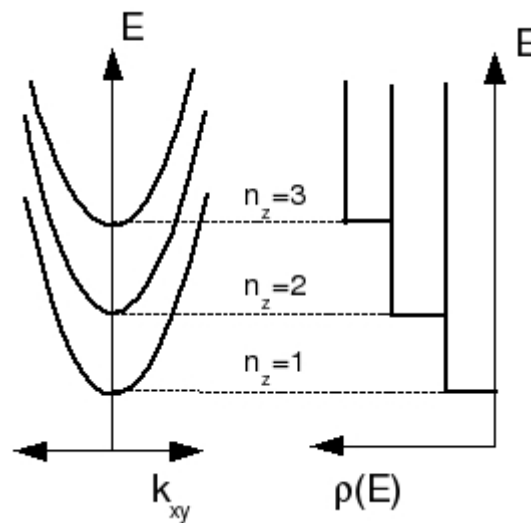


Figure 2.13: On the left, the parabolic band structure for an infinite quantum well is plotted, on the right the 2D-density of states is plotted.

2.4 Lasing threshold

As the p-n junction is forward biased and the current increases, more carriers are

captured into the confined states of the QW. When the carrier density in the QW is high enough for population inversion to be achieved and the gain is high enough to overcome the material losses the medium is said to have become transparent. As the carrier density is further increased, the gain becomes high enough to overcome all cavity losses (including the mirror losses) - this point is called threshold (I_{th}). An L-I curve is plotted in figure 2.14. The emission spectra that would be observed at the front facet of the laser is shown in figure 2.15. Far below threshold (a), only spontaneous emission is observed. As the threshold condition is approached, the spontaneous emission spectrum is amplified by the stimulated emission processes, forming the true amplified spontaneous emission spectrum (ASE). The cavity superimposes (modulates) its resonances on top of the true ASE spectrum forming a comb-like spectrum. From this modulated ASE spectrum, it is possible to calculate the optical gain [8]. Ideally far above threshold a signal mode dominates the lasing spectra. However, in practice effects such as spectral hole burning mean that often more than one mode can lase.

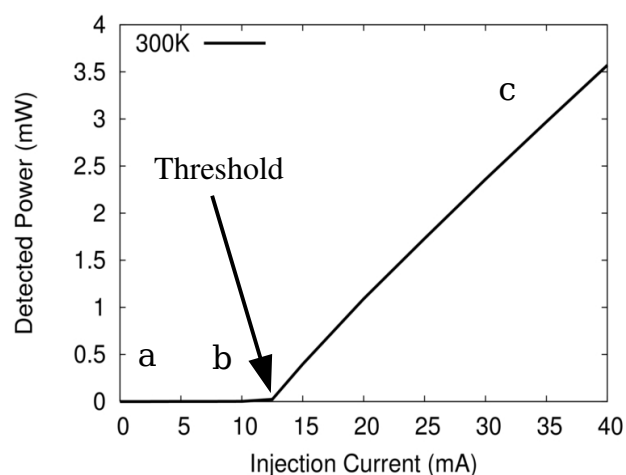


Figure 2.14: Typical LI-curve.

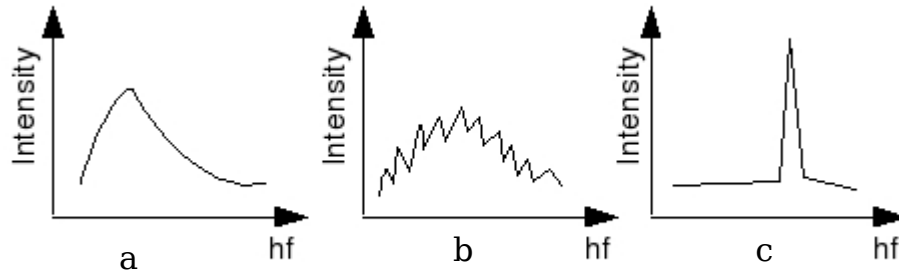


Figure 2.15: Emission spectra (a) far below threshold (b) just below threshold (c) far above threshold [2].

2.5 Dark recombination processes

Radiative recombination processes are not the only processes in semiconductors. There are also dark recombination processes, which produce no light. The main dark recombination processes in semiconductors at room temperature are the Shockley-Read-Hall (SRH) and Auger recombination processes. SRH describes the recombination of electrons (in the conduction band) and holes (in the valance band) through defect states within the band gap. The energy $E_e - E_h$ is released to the lattice. The recombination rate is

$$R^{SRH} = \frac{(np - n_i^2)}{\tau_{p0}(n + n_i) + \tau_{n0}(p + n_i)} \quad , \quad (2.35)$$

where the lifetimes τ_{p0} and τ_{n0} are the recombination lifetimes for electrons and holes. [9]

Auger recombination is a three body process involving either two electrons and a hole or two holes and an electron, in which one electron and one hole recombine. The

excess energy ($E_c - E_h$) is given to the extra electron or hole. The recombination rate is phenomenologically described by [9]

$$R^{Auger} = (C_n n + C_p p)(np - n_i^2) \quad , \quad (2.36)$$

where C_n and C_p are the Auger recombination parameters for electrons and holes respectively.

2.6 Laser structures

2.6.1 Ridge waveguide structures

The first lasers produced were broad area structures, which provided no lateral confinement for the optical mode. Broad area devices can produce very high powers [10], but are susceptible to filamentation and have poor beam quality. This makes coupling to fibres difficult. Such a device is depicted in figure 2.16.

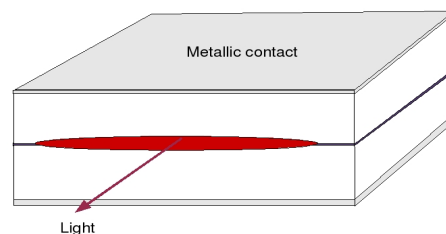


Figure 2.16: Broad area structure.

An optical ridge waveguide can be defined by etching two trenches. This enables lateral mode confinement and improves the beam quality, thereby making it easier to couple the light into a single-mode optical fibre.

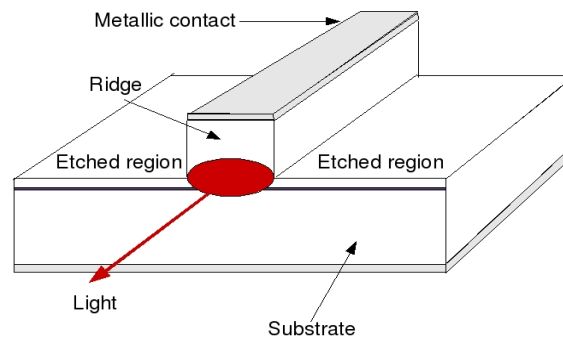


Figure 2.17: Ridge waveguide structure.

High power 980nm RW structures optimised for the pumping of EDFAs have been shown capable of delivering up to 1.8W of optical power [11]. However, due to the tightly confined mode and high optical power, it is possible to damage the front facet (i.e. catastrophic optic damage). Short haul low power 1.1 μ m RW lasers have shown capable of modulation rates up to 40GHz [12].

2.6.2 Tapered laser structures

Although ridge waveguide lasers have been shown capable of producing 1.8W [11] of optical power, tapered lasers have been shown capable of producing nearly-diffraction limited beams in excess of 6.7W [13-14]. A tapered laser consists of two functional blocks - the ridge waveguide (RW), and the tapered section (figure 2.18). The ridge waveguide serves two purposes. Firstly, it provides a single lateralspatial mode to the tapered section of the laser, and secondly, it filters out the higher order lateral modes returning from the waveguide. The tapered region amplifies the small input power from the RW section to produce a large output power. The tapered region allows the

light to diffract out as it propagates towards the front facet, thus reducing its power density and reducing the risk of saturation, spatial hole burning, self focussing, and catastrophic optical damage [15].

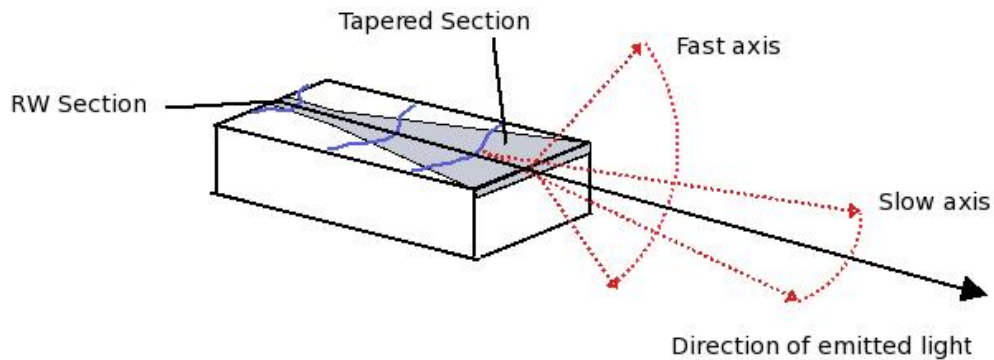


Figure 2.18: A pictorial example of light progressing down the RW structure and being amplified in the tapered section. The fast and slow optical axes have been marked.

2.6.3 Vertical Cavity Surface-Emitting Lasers (VCSELs)

Edge emitting lasers (EELs) were the first class of diode laser to be developed. The light produced by a typical EEL is highly divergent and astigmatic. The beam diverges very quickly along the vertical axes. However, along in the horizontal axis, the beam diverges slowly. This is due to diffraction. (see figure 2.18) It is usual to use complex corrective optics to focus the light into a non-divergent beam.

The vertical cavity surface emitting laser or VCSEL is another class of laser which emits light normal to the epitaxial layers. Due to the circular beam, the coupling optics are much simpler, making coupling into a fibre less costly. Cost is also reduced in this class of device for two reasons. Foremost, a very high number of devices can be grown per wafer and secondly no packaging is required to test the

operation of the device [16]. Thus, resources are not spent packaging broken structures. The structure can be integrated into 2D arrays. VCSELs also have very low threshold and operating currents, but have a limited output power.

2.6.4 Other laser structures

Many other variations of the basic laser diode have been proposed. By reflecting light from the laser back into the cavity, the beam quality can be significantly altered [17], [18],[19]. The effects can be both positive and negative, causing either constructive or destructive interference [17], frequency stabilization [19], or even hysteresis [17]. Distributed feedback lasers (DFB) are another class of specialised laser, designed to have a very stable wavelength. A stable lasing wavelength is achieved by etching a Bragg grating along the structure close to the active region. DFB lasers are commonly used [20] for DWDM applications where frequency stability is essential. A very different and more complex type of laser diode is the quantum cascade laser (QCL). Unlike other laser diodes, which rely on a conduction-valance band transition to generate photons, QCLs are unipolar. Photons are generated via intersubband transitions between the conduction subbands of a superlattice [21]. This allows far infra-red emission to be achieved.

2.7 Lifetime, degradation and heat

High heat dissipation rates are inescapable with the ever increasing need for higher power and higher speed devices. With higher heat dissipation, comes higher temperature and faster degradation rates [22-24]. Indeed, a well known technique to

accelerate device ageing is to run the device at higher temperatures [25]. Active cooling of high power devices is often used to achieve high power operation along with long lifetime. However, active cooling increases power consumption, device complexity and total unit cost. In order to achieve the long lifetimes required by the telecommunications industry, laser structures must be optimised optically, electrically and thermally.

In order to increase device performance whilst maintaining long lifetime, a good understanding of the dominant heat generation mechanism is required. A cost effective way to gain such an understanding is with the use of predictive device models. One of the key model parameters required for accurate simulation is optical gain. In the next chapter, a study of optical gain in 1.3 μm dilute nitride double quantum well laser diodes is performed.

2.8 References

- [1] H.C. Casey, J.P. and M.B. Panish “Heterostructure Lasers Part A: Fundamental Principles” Quantum Electronics Principles and Applications”, ISBN: 0-12-163101-X, Academic Press Inc, 1978
- [2] Streetman B.G., “Solid state Electronics Fifth Edition”, ISBN: 0130255386, Prentice Hall Press, 1999
- [3] Agrawal and Dutta “Semiconductor Lasers Second Edition”, ISBN: 0-442-01102-4, Van Nostrand Reinhold Press, 1993

- [4] S. Bull, "Photo- and Electroluminescence Microscopy and Spectroscopy Investigations of High Power and High Brightness Semiconductor Laser Diodes", PhD Thesis, University of Nottingham, September 2004.
- [5] P. Harrison "Quantum Wells, Wires and Dots Theoretical and Computational Physics", ISBN: 978-0-470-01079-2 , John Wiley and Sons, Lt,
- [6] Sara M. McMurry "Quantum Mechanics" Addison Wesley Longman ISBN-10: 0201544393, ISBN-13: 978-0201544398, 2005
- [7] P.S. Zory J.R, "Quantum Well Lasers", ISBN: 0-12-781890-1, Academic Press , 1993
- [8] B. W. Hakki, T. L. Paoli, "Gain spectra in GaAs double-heterostructure injection lasers", Journal of Applied Physics, 46, pp. 1299-1306, 1975
- [9] Joachim Piprek, "Semiconductor Optoelectronic Devices Introduction to Physics and Simulation ", ISBN: 0125571909, Academic Press , 2003
- [10] A. Al-Muhanna, L. J. Mawst, D. Botez, D. Z. Garbuzov, R. U. Martinelli, and J. C. Connolly, "14.3 W quasicontinuous wave front-facet power from broad-waveguide Al-free 970 nm diode lasers," *Appl. Phys. Lett.*, vol. 71, pp. 1142–1145, 1997
- [11] N. Lichtenstein, B. Schmidt, A. Fily, S. Weiß, S. Arlt, S. Pawlik, B. Sverdlov, J. Müller, C. Harder, "DPSSL and FL Pumps Based on 980nm-Telicom Pump Laser Technology: Changing the Industry", 2nd conference on high-power diode lasers technology and applications San Jose, Ca., PROC SPIE, 5336 , p.77-83

- [12] S. Weisser, E.C. Larkins, K. Czotscher, W. Benz, J. Daleiden, I. Esquivias, J. Fleissner, J.D. Ralston, B. Romero, R.E. Sah, A. Schonfelder, J. Rosenzweig, "Damping-limited modulation bandwidths up to 40 GHz in undoped short-cavity $\text{In}_{0.35}\text{Ga}_{0.65}\text{As}$ -GaAs multiple-quantum-well lasers" *IEEE Photonics Technology Letters*, 8, 5, pp. 608-610, 1996
- [13] G. Erbert, J. Fricke, R. Huelsewede, A. Knauer, W. Pittoff, P. Ressel, J. Sebastian, B. Sumpf, H. Wenzel and G. Traenkel, "3-W high brightness tapered diode lasers at 735 nm based on tensile-strained GaAsP QWs", *Proc. SPIE 4995*, 2003
- [14] K. Paschke, B. Sumpf, F. Dittmar, G. Erbert, J. Fricke, A. Knauer, S. Schwertfeger, H. Wenzel and G. Trankle "Nearly-diffraction limited 980 nm tapered diode lasers with an output power of 6.7 W" *2004 IEEE 19th International Semiconductor Laser Conference, Conference Digest*, pp. 43-44, 2004
- [15] S. Delépine, P. Salet, F. Gérard, A. Pinquier, T. Fillion, J. Pasquier, P. Doussièrè, J.-P. Chardon, M. DiMaggio, F. Boubal, G. Gelly, "370mW coupled into single mode optical fibre from 1.48 μm unstable cavity laser", *Electronics Letters*, 35, 2, pp. 145-146, 1999
- [16] C.W. Wilmsen, H. Temkin, L. A. Coldren "Vertical-Cavity Surface-Emitting Lasers", ISBN 0521006295, Cambridge University Press, 1999
- [17] R. Lang and K. Kobayashi "External Optical feedback Effects on Semiconductor Injection Laser Properties" *IEEE Journal of Quantum Electronics*, 16, 3, p. 347, 1980

- [18] A.P Bogatov, P.G. Eliseev, L.P. Ivanov, A.S. Logginov, M.A. Manko and K. YA Senatorov "Study of the Single-Mode Injection Laser", IEEE Journal of Quantum Electroics, 9, 2, p.392-394, 1973
- [19] N. Chinone, K. Aiki and R. Ito "Stabilization of semiconductor laser outputs by a mirror close to a laser facet" Appl. Phys. Lett., 33, 12, p.993, 1978
- [20] John E. Carroll, James Whiteaway, Dick Plumb "Distributed Feedback Semiconductor Lasers" IET Publishing ISBN 0852969171,1998
- [21] Hong Kyun Choi, "Long-Wavelength Infrared Semiconductor Lasers", ISBN 0471392006, Wiley-IEEE, 2004
- [22] A. Kozłowska, M. Latoszek, J. Tomm, F. Weik, T. Elsaesser, B. Spellenberg and M. Bassler, "Analysis of thermal images from diode lasers: Temperature profiling and reliability screening", App. Phys. Lett., 86, 203503, 2005
- [23] A. Kozłowska and P. Wawrzyniak, J. W. Tomm, F. Weik, and T. Elsaesser, "Deep level emission from high-power diode laser bars detected by multispectral infrared imaging", Applied Physics Letters, 87, 153503, 2005
- [24] T. Tien, F. Weik, Jens W. Tomm, B. Sumpf, M. Zorn, U. Zeimer, and G. Erbert "Thermal properties and degradation behavior of red-emitting high-power diode lasers" Appl. Phys. Lett. 89, 181112, 2006
- [25] Kenji Endo, Kennichi Kobayashi, Hiroaki Fujii, and Yoshiyasu Ueno "Accelerated aging for AlGaInP visible laser diodes" Appl. Phys. Lett. 10, 64, 2, pp.

146-148, 1994